IEEE Open Journal of
Power Electronics

Received 21 June 2022; revised 14 July 2022; accepted 25 July 2022. Date of publication 29 July 2022;
date of current version 10 August 2022. The review of this article was arranged by Associate Editor Cheng (OJ GAE) Wang.

Digital Object Identifier 10.1109/OJPEL.2022.3194849

Grid Strengthening IBR: An Inverter-Based Resource Enhanced by a Co-Located Synchronous Condenser for High Overcurrent Capability

HAIGUO LI [1] (Member, IEEE), CHENG NIE [2] (Member, IEEE), AND FRED WANG [1,3] (Fellow, IEEE)

[1]Min H. Kao Department of Electrical Engineering and Computer Science, The University of Tennessee, Knoxville, TN 37996 USA
[2]TBEA CO., Ltd., Xi'an 710000, China
[3]Oak Ridge National Laboratory, Oak Ridge, TN 37830 USA

CORRESPONDING AUTHOR: HAIGUO LI (e-mail: hli96@vols.utk.edu)

This work was supported primarily by the Engineering Research Center Program of the National Science Foundation and the Department of Energy under NSF Award Number EEC-1041877 and the CURENT Industry Partnership.

ABSTRACT With the increasing penetration of inverter-based resources (IBRs) and the standing down of synchronous generator-based resources (SGBRs), some IBRs, at least, need to provide grid support functions commonly provided by SGBRs. IBRs usually have a much smaller overcurrent capability than SGBRs, which can result in weak grid strength and corresponding issues on grid transient voltage support, system protection, and black start. This paper aims at addressing the low overcurrent capability issue of IBRs from the source side by combining an IBR with a co-located synchronous condenser (SC). Dubbed grid strengthening IBR (GSI), the proposed setup in grid forming mode uses the SC to regulate the terminal voltage and the IBR to regulate the frequency. The proposed GSI is evaluated through its comparison with an SGBR in the single-unit operation considering different grid faults, multi-unit operation, and transient stability performance. It is verified that the GSI can provide an overcurrent and maintain the terminal voltage comparable to or even slightly better than the SGBR during grid faults. The GSI does not have any transient stability issues; even after a long fault period, it can reestablish the system synchronism. The GSI can help the penetration of the IBRs in the system, as the system operation and the system loads will be largely unaffected, even during transients.

INDEX TERMS Grid strengthening inverter-based resources, synchronous condenser, synchronous generator, overcurrent capability, transient stability, voltage support.

I. INTRODUCTION

Due to the energy crisis and environmental problems, inverter-based resources (IBRs), such as PV and wind, are increasingly used in power grids, including microgrids [1]. At the same time, the conventional synchronous generator-based resources (SGBRs) are gradually standing down. As a result, IBRs need to provide grid support functions normally provided by SGBRs, such as voltage and frequency regulations [2]. These IBRs are dubbed grid forming (GFM) inverters, to differentiate from grid following (GFL) inverters, which rely on the external grid voltage generally provided by conventional SGBRs.

Since GFM IBRs are to replace SGBRs, it is desirable or even necessary for them to perform all the positive system functions of SGBRs such that the system can still operate. For SGBRs, all these functions are realized through the characteristics and control of synchronous generators (SGs), prime movers, and associated energy sources (e.g., fuel for turbines). Similarly, most of these functions can be realized through characteristics and proper control of the GFM inverters and associated energy resources (e.g., wind, solar, and battery). For example, voltage and frequency control of GFM IBRs can be realized through several control methods, such as droop control and virtual synchronous generator (VSG) control [3],

[4]. Even inertia, which is an intrinsic characteristic of rotating machines but not for static inverters, can be well emulated by the GFM IBRs with proper energy reserve or storage [5]–[8]. With the flexibility of inverters and their fast active and reactive power control, GFM IBRs can be programmed to behave similar to or even better than their SGBR counterparts in many cases.

One significant characteristic that is difficult for an IBR to achieve is the overcurrent capability. The commercially available inverters only provide an overcurrent of less than 2 p.u. [1], [2], while the SGs can provide more than 5 p.u. [9]. The overcurrent characteristic is critical for the power system operation and load support. A low overcurrent capability will result in weak grid strength and many corresponding issues, of which the three main ones are discussed as follows.

1) The low overcurrent capability impacts the system voltage support during transients, such as grid faults and large load changes. During the same transient, due to the current limit, the grid voltage supported by the GFM inverter will be lower than that by the SG. As a result, some loads may trip or fail to start, since these loads require a sufficient voltage to start (such as a motor) or are designed to ride through the grid transient based on existing grid voltage (or power quality) standards, such as the Information Technology Industry (ITI) curve [10] and the IEEE Std 1668 [11].
2) The low overcurrent capability impacts the power system protection [1], [2], [12]. The existing overcurrent-based system protection devices cannot be triggered by low fault currents. Although the threshold values of these system protection devices can be adjusted, the distinction between faults and certain normal transients, such as motor starting and transformer energization, will become difficult. There have been some adaptive protection methods proposed for the microgrid to address this issue [13], [14]. For the large power system with high penetration of IBRs, more complex fault detection and protection schemes are needed, such as traveling wave-based methods [15].
3) The low overcurrent capability affects the system restoration, known as "black start". To accomplish the black start, high inrush currents are needed to energize system equipment, such as transformers, and support loads like motors. With limited current, GFM inverters may fail to start the system or support loads. As shown in [16], with a 10 p.u. current limit, the IBR-based system can be started within 2 seconds, and the voltage can be maintained at 0.95 p.u. or even higher. However, with a 1.2 p.u. current limit, the system cannot be started with a loaded induction motor; with an unloaded induction motor, it can be eventually started after more than 20 seconds, while the voltage during the starting process is only 0.3 p.u.

The low overcurrent capability has also been found to potentially cause system transient stability issues [17], which can be largely avoided with improved control methods [18]–[20]. Among the three main issues discussed above, the protection issue may be eventually solved by advanced protection methods; however, significant changes will be needed for both the system and the loads, which will be difficult. The transient voltage support and black start affect loads, so the source side, system-level, and/or load side solutions are needed. Nevertheless, it is difficult to implement changes to existing system loads, so the system-level solution is mostly used now.

Synchronous condensers (SCs) have been used in the power system for a long time to provide reactive power, inertia, and short circuit current [21], [22]. As the penetration of IBR increases in the power system, the employment of SC somewhere in the system is also a solution to address the issues brought by IBRs. It is studied that SCs provide inertia and large short-circuit current during grid faults, improving the system frequency and voltage performances [23]–[27]. In addition, the SC improves the transient stability of the power system with GFL inverters [28]. However, these SCs are mostly installed and operated in the system, independent of sources or loads; and the system-level analysis and control are needed to size the SCs and evaluate their performances, which makes it complicated. Although the SC siting optimization, in terms of the SCR improvement and cost, is considered in [29], [30], as the system becomes large, the solution will become more difficult.

Therefore, a solution from the grid source side, which provides IBRs with the transient overcurrent comparable to SGBRs, is desirable. Based on this, each IBR can be treated similarly to an SGBR, and the conventional system design approaches can also be used. However, this is rarely discussed in the literature to the best of the author's knowledge.

This paper aims at addressing the overcurrent capability issue of GFM IBRs from the source side. A grid strengthening IBR (GSI), combining an IBR with a co-located SC, is proposed to achieve a similar overcurrent capability of SGBRs, such that the GSI can perform similar to an SGBR, and many issues caused by the low overcurrent capability, such as the three discussed above, can be solved. A comparison study between the proposed GSI and the SGBR is conducted in steady-state operation, fault conditions with different fault types and fault impedances, multiple-unit operation, and transient stability performance.

The rest of the paper is organized as follows. In Section II, the proposed GSI and its control are introduced. Then, the performance comparison between the GSI and an SGBR in terms of the single-unit operation considering both steady-state and fault conditions, multiple-unit operation, and transient stability are presented in Sections III, IV, and V, respectively. In Section VI, some discussions about possible future work are given. Finally, Section VII concludes this paper.

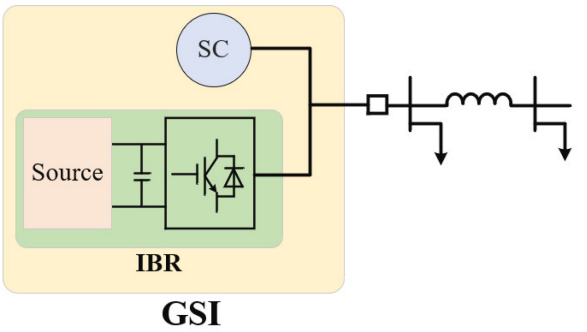

FIGURE 1. Configuration of the proposed GSI.

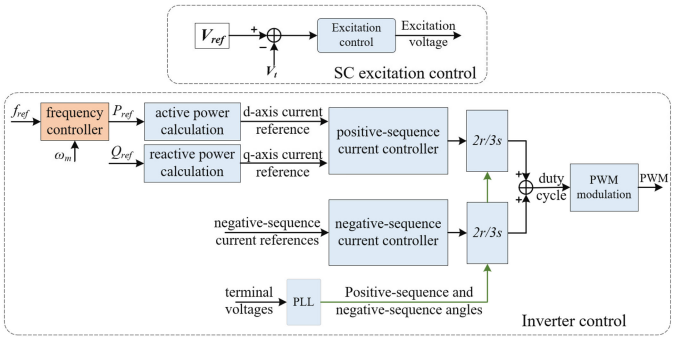

FIGURE 2. The control structure of the proposed GSI.

II. THE PROPOSED GSI AND ITS CONTROL

A. THE PROPOSED GSI SETUP AND CONTROL

The wound-field synchronous machine (WFSM) used for SCs and SGs is currently the most suitable technology to provide high overcurrent capability. The WFSM is electromechanical and electromagnetic in nature with high thermal capacity, and therefore can carry large transient overcurrent without exceeding its temperature limits, unlike power electronics equipment. Other devices that can produce high and fast-rising overcurrent in ac systems include ac capacitor banks and transformers. Ac capacitor banks rely on voltage change to generate current and would require extremely large capacitance to hold the voltage. Besides, the capacitor bank voltage and current are difficult to control without additional series devices, like power electronics switches that lack overcurrent capability. The issue with the transformer is that when its primary winding is producing a high overcurrent, its secondary winding needs to provide a corresponding current, as well as an ac voltage source. With today's technology, the ac source can only be inverter-based or synchronous machine-based. So, the transformer approach is not attractive. As a result, this paper chooses to use the SC to work with the IBR to realize the proposed GSI. If other more cost-effective devices with high overcurrent capability become available in the future, they could substitute the SC in the GSI setup.

The proposed GSI setup is shown in Fig. 1. It consists of an IBR and an SC with their ac terminals connected to the same bus. The IBR has a relatively low current limit, and the SC is responsible for providing the overcurrent during the transient. Different from previous applications where the SC is used independent of IBRs, in the GSI setup, the SC and the IBR are treated as one unit. They work together to control the terminal voltage and frequency, similar to a conventional SGBR unit.

The control structure of the GSI in grid forming mode is shown in Fig. 2, consisting of the SC excitation control and the inverter control. The terminal voltage magnitude, V_t, of the GSI is controlled to its reference, V_{ref}, through the SC excitation control. The inverter control structure is realized in the dq synchronous frame, and the d-axis is selected to align in phase with the terminal voltage through a phase-locked loop, similar to the GFL inverter case. Different from the GFL inverter, which regulates active and reactive power, this inverter controls the SC mechanical speed, ω_m, which is corresponding to the terminal voltage frequency, f_t, through active power control. Therefore, the voltage and frequency control functions of the GSI are divided into two separate parts and are handled by the SC and the IBR, respectively.

Different approaches can be used to generate the frequency reference, f_{ref}, and two of them are introduced here. One is a given constant value, which can be used in an autonomous system or an islanded microgrid with one source unit, where no power sharing is needed. The other one is to generate the frequency reference through the active power sharing control, for example, the droop control. In this paper, in the single-unit operation, the frequency reference is given a constant value, i.e., 60 Hz; and in the multi-unit operation, the droop control is used to generate the frequency reference.

The inverter controller includes the outer frequency loop and inner current loop. The frequency loop acts on the frequency reference, f_{ref}, and the SC mechanical speed to generate the active power reference, P_{ref}, which is further used to calculate the positive-sequence d-axis current reference. The reactive power reference, Q_{ref}, is used for the positive-sequence q-axis current reference calculation, and it is controlled to be zero in this paper. The d-axis and q-axis current references are given to the inner current loop controllers, which are similar to typical GFL inverter control [31], [32].

The inverter controller also includes the negative-sequence control, which only has the current loop. In this paper, the negative-sequence d-axis and q-axis currents are controlled to be zero, so that the negative-sequence current, if any, will be provided by the SC, which is also similar to the situation of the SGBR. On the other hand, the inverter can be controlled to provide a negative-sequence current per system needs to reduce the thermal and mechanical stress of the SC caused by the negative-sequence current [33].

B. THE INVERTER FREQUENCY CONTROLLER

The main difference between the GSI inverter and the conventional GFL or GFM inverter is the frequency controller. The GSI inverter does not directly generate the terminal voltage frequency or angle. Instead, it controls the frequency indirectly by controlling its active power output.

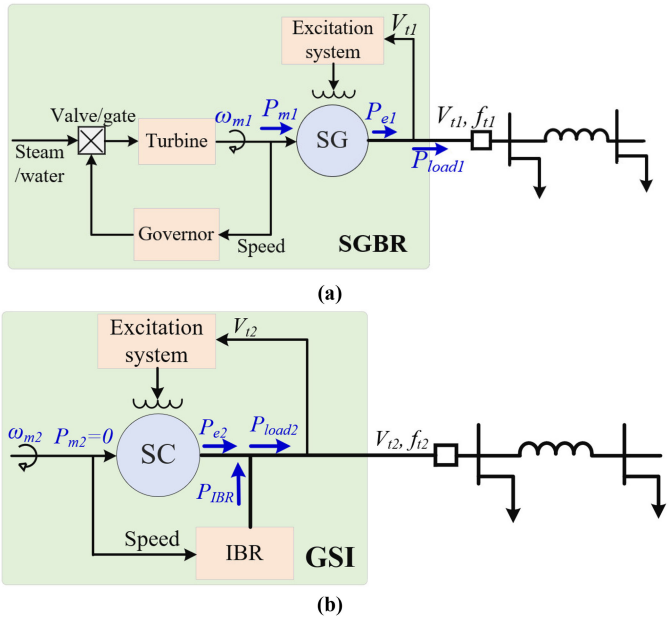

FIGURE 3. The control diagram of (a) the SGBR [34] and (b) the GSI.

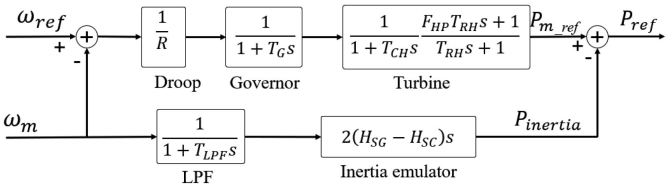

FIGURE 4. The governor and turbine mode for the inverter frequency controller.

The inverter active power in the GSI acts as the mechanical power in the SGBR. The high-level power, speed, excitation, and voltage relationships of the SGBR [34] and the GSI are shown in Fig. 3(a) and (b), respectively. Both the SGBR and the GSI use an excitation system to control the terminal voltage magnitude. The SGBR utilizes the prime mover (turbine) and the governor to control the frequency through controlling the SG mechanical power input, P_{m1}. Since the SC mechanical power input, P_{m2}, is zero, the GSI uses the IBR to control the frequency by controlling the IBR electrical power output, P_{IBR}. The mechanical equation of the SG is

$$J_1\omega_{m1}\frac{d\omega_{m1}}{dt} + D_1\omega_{m1} = P_{m1} - P_{e1} - P_{Loss1} = P_{m1} - P_{load1}(v_{t1}, f_{t1}) - P_{Loss1} \quad (1)$$

and the mechanical equation of the SC is

$$J_2\omega_{m2}\frac{d\omega_{m2}}{dt} + D_2\omega_{m2} = P_{m2} - P_{e2} - P_{Loss2} = P_{IBR} - P_{load2}(v_{t2}, f_{t2}) - P_{Loss2} \quad (2)$$

where subscripts *1* and *2* denote the parameters for the SG and SC, respectively; J is the moment of inertia; ω_m is the mechanical speed; D is the coefficient to account for mechanical friction and windage (F&W); P_m is the mechanical power input; H is the inertia constant; P_e is the electrical power output; P_{IBR} is the inverter active power output; P_{load} is the total system load power, which may have a relationship to the terminal voltage and frequency; and P_{Loss} is the electrical loss of the SG or SC.

When the GSI and the SGBR have the same performances: the same terminal voltage and frequency, the power consumed by the system loads are the same, which means

$$P_{load1}(v_{t1}, f_{t1}) = P_{load2}(v_{t2}, f_{t2}) \quad (3)$$

Substituting (1) and (2) into (3) yields

$$P_{m1} - P_{Loss1} - J_1\omega_{m1}\frac{d\omega_{m1}}{dt} - D_1\omega_{m1} = P_{IBR} - P_{Loss2} - J_2\omega_{m2}\frac{d\omega_{m2}}{dt} - D_2\omega_{m2} \quad (4)$$

Then, to get $\omega_{m1}=\omega_{m2}=\omega_m$, the inverter output power P_{IBR} needs to be

$$P_{IBR} = P_{m1} - (J_1 - J_2)\omega_m\frac{d\omega_m}{dt} - (D_1 - D_2)\omega_m - (P_{Loss1} - P_{Loss2}) \quad (5)$$

In (5), the first term on the right side is the mechanical power input of the SG, which is corresponding to the active power regulation of the turbine and governor; the second term is used to compensate for the inertia difference between the SGBR and the SC; and the third and fourth terms compensate for the F&W loss and electrical loss differences respectively, which are small and therefore neglected in the following analysis.

1) GOVERNOR AND TURBINE EMULATOR IMPLEMENTATION

The straightforward approach to realize (5) is to use a governor and turbine emulator. Based on [34], the inverter frequency controller model, which is based on per-unit values, is developed, as shown in Fig. 4. First, the terminal voltage frequency reference is converted to the mechanical speed reference, ω_{ref}. Then, the difference between the reference and the feedback is given to the governor and turbine model to generate the mechanical power reference, P_{m_ref}. To minimize the noise impact, a low pass filter (LPF) is adopted in the inertia emulator loop. The total active power reference is the combination of P_{m_ref} and the inertia emulator output, $P_{inertia}$.

2) PI CONTROLLER IMPLEMENTATION

However, it is not necessary to have the frequency controller emulating the governor and turbine. Besides, the active power control of the governor and turbine is slow, which makes the frequency regulation speed slow. The inverter, however, has a very fast active power control capability, and it will benefit the frequency control.

The GSI control model with the governor and turbine emulator is shown in Fig. 5. When the part in the red dashed box is

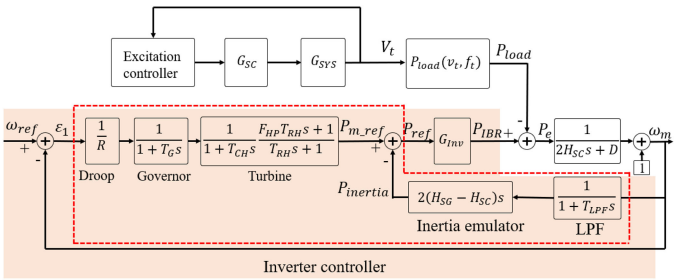

FIGURE 5. The GSI control model with governor and turbine emulator-based frequency controller.

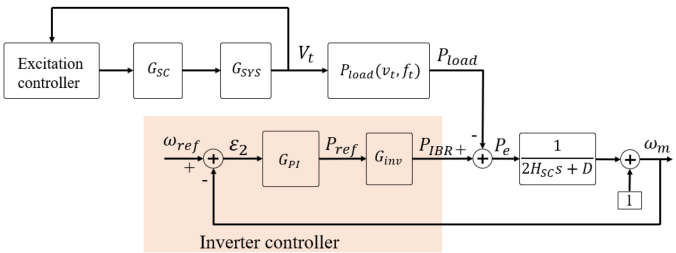

FIGURE 6. The GSI control model with PI-based frequency controller.

replaced with a PI controller it becomes Fig. 6. The open-loop transfer function from the mechanical speed error, $\varepsilon_1/\varepsilon_2$, to the mechanical speed, ω_m, of the two control methods are respectively

$$\frac{\omega_m}{\varepsilon_1} = \frac{\frac{1}{R}\cdot\frac{1}{1+T_G s}\cdot\frac{1}{1+T_{CH}s}\cdot\frac{F_{HP}T_{RH}s+1}{T_{RH}s+1}\cdot G_{inv}\cdot\frac{1}{2H_{SC}+D}}{1+G_{inv}\cdot\frac{1}{2H_{SC}+D}\cdot\frac{2(H_{SG}-H_{SC})s}{1+T_{LPF}s}} \quad (6)$$

and

$$\frac{\omega_m}{\varepsilon_2} = G_{PI}\cdot G_{inv}\cdot\frac{1}{2H_{SC}+D} \quad (7)$$

where the inverter transfer function, G_{inv}, is considered to be a time delay corresponding to the current-loop control bandwidth.

The bode plot comparison between the two transfer functions is shown in Fig. 7. In the governor and turbine emulator-based control, the bandwidth is around 0.1 Hz due to the slow governor and turbine response speed. However, with the PI controller-based control, the bandwidth is improved to around 100 Hz considering the same phase margin.

3) COMPARISON BETWEEN THE TWO IMPLEMENTATIONS

A simulation comparison between the two implementations of the GSI and the SGBR is carried out with MATLAB/Simulink, considering both steady-state and transient operations.

An identical WFSM is used for both the SG and the SC. The Simulink sixth-order state-space-based synchronous machine model, considering both the sub-transient and transient conditions, is used. Parameters of a real 625 kVA WFSM used in a microgrid are employed in the SG and SC models, and the values are shown in Table 1. The only difference between the

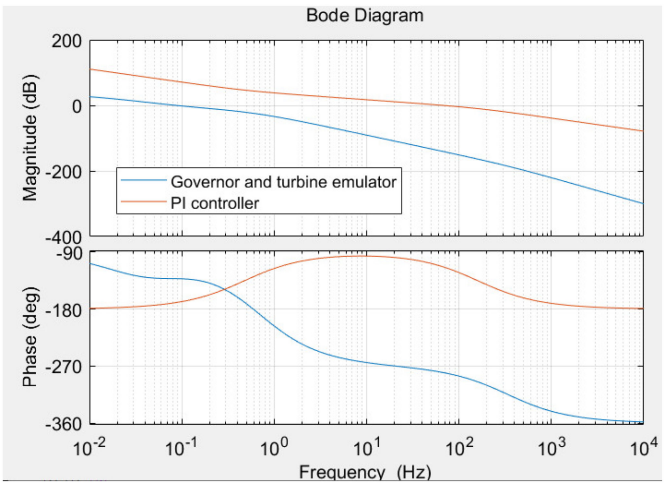

FIGURE 7. The bode plot comparison between the governor and turbine emulator-based control and the PI controller-based control.

TABLE 1. WFSM, Governor, and Turbine Parameters

Parameters	Values	Parameters	Values
Voltage (V)	480	Power rating (kVA)	625
Xd (p.u.)	3.4375	Xd' (p.u.)	0.2626
Xd" (p.u.)	0.1836	Xq (p.u.)	1.7499
Xq" (p.u.)	0.1790	Xl (p.u.)	0.07
Td' (s)	0.1832	Td" (s)	0.0069
Tqo" (s)	0.0069	Rs (p.u.)	0.0331
H (s)	SG: 7 SC:1.1	R	0.05
T_G	0.2	T_{CH}	0.3
F_{HP}	0.3	T_{RH}	7.0
D	0	p	1

SC and SG model parameters is the inertia constant. Based on [35], the typical inertia constant of an SG together with the turbine is in the range of [6 s, 9 s], and the range for SC is [1.0 s, 1.25 s]. To accommodate relatively large machines, in this paper, inertia constant values of the SC and SGBR are assumed to be 1.1 s and 7.0 s, respectively. The AC1A excitation model in IEEE Std 421.5-2016 [36] is used for both the SG and SC, controlling the terminal voltage to be the reference. The SGBR also has a turbine and governor model, controlling its mechanical speed to the rated speed, corresponding to the frequency reference. Because the per-unit values are used, the work can be extended to larger machines.

The inverter switching model is adopted, and the main parameters are shown in Table 2. The front-end source and the energy storage are simplified, and they are represented by a constant dc source. Their response time/speed may impact the GSI performances, which will also be considered later in this paper.

To compare the control performance, the inverter does not have a current limit. The fault is triggered at 5 s and lasts for 10 cycles. The voltage and frequency comparison between the two frequency control methods of GSI and the SGBR in the three-phase fault is shown in Fig. 8. The GSI with a

TABLE 2. Inverter Parameters

Parameters	Value
Topology	Three-phase two-level voltage source converter
DC-link voltage	1 kV
AC filter (LCL)	Inverter-side inductor: 0.03 p.u. Capacitor: 0.026p.u. Grid-side inductor: 0.03p.u. Damping resistor: 0.1 Ω(0.43p.u.)
Switching frequency	10 kHz

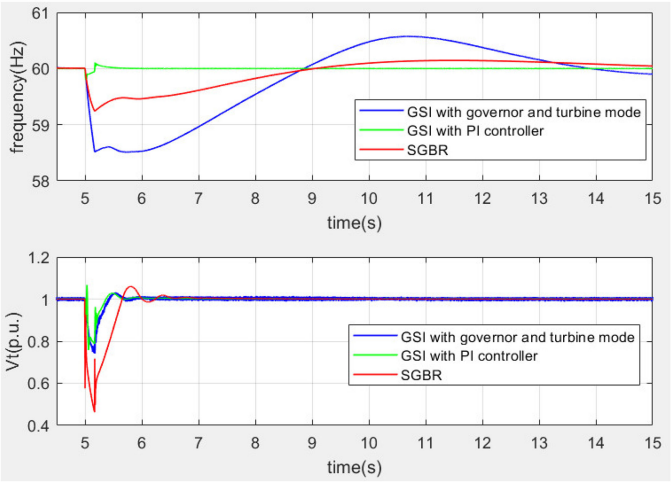

FIGURE 8. Frequency and voltage performance comparison among the GSI with governor and turbine model, GSI with PI controller, and the SGBR in a three-phase fault condition.

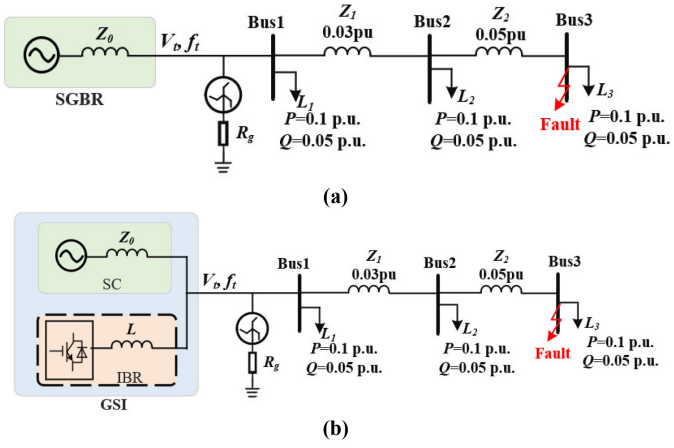

FIGURE 9. Single-unit operation configuration of (a) the SGBR case and (b) the GSI case.

PI-based frequency controller (the green curve) has the smallest frequency change during the fault period, and the fastest frequency recovery speed after the fault is cleared because of the fast active power control.

Compared to the SGBR, the GSI with governor and turbine mode (the blue curve) has a lower frequency nadir, larger frequency variation, and longer frequency recovery period. Because of the current contribution of the inverter, the SC provides less fault current than the SG. Since the internal voltage drop is smaller in the SC than in the SG, the terminal voltage is higher. However, since resistive loads are assumed, the GSI has to provide more active power. Because of the slow active power regulation speed of the inverter in the governor and turbine emulator mode, part of the active power comes from the SC kinetic energy, which slows the SC down, resulting in a frequency drop.

Therefore, using the PI controller as the frequency controller is better than using the governor and turbine emulator. In the following analysis, the PI controller-based frequency controller is adopted. However, with the current limit, the maximum inverter active power output will be limited. Then, the SC needs to provide active power, and the frequency nadir will be lower. This will be discussed in the next Section.

III. SINGLE-UNIT OPERATION

To fully verify the proposed setup and control, the GSI and the SGBR are further compared in different conditions. In this section, the comparison is conducted in the single-unit operation condition, considering the steady-state operation and faults. As shown in Fig. 9(a) and (b), the SGBR or the GSI is connected to a simple radial distribution system, and a zig-zag grounding transformer is used to provide the grounding for the system. The transformer grounding resistance is 0.01 p.u., and the three loads are the same: 0.1 p.u. active power and 0.05 p.u. reactive power. Also, from now on, the converter current limit is set at 1 p.u.

A. STEADY-STATE OPERATION

The steady-state operation comparison is first conducted. As shown in Fig. 10(a), in the SGBR case, the SG provides all the load current. In the GSI case, as shown in Fig. 10(b), the SC and the inverter share the load current. The SC provides the reactive power, and the inverter provides the active power, which can be observed from the phase angle difference between the voltage and current waveforms. Because of the high-frequency switching of the power electronics inverter, the GSI terminal voltage has harmonics. The GSI terminal voltage harmonic spectrum is shown in Fig. 11. The total harmonic distortion (THD) is calculated, considering up to 50^{th}-order based on IEEE Std. 519-2014, to be 2.92%, which meets the requirement [37]. Also, the individual harmonic, as shown in Fig. 11, meets the requirement. The high-frequency harmonics are mainly at the switching frequency and its multiplier. It is difficult for the high-frequency harmonics to spread away in the power system since they are damped by the line resistance at high frequency or filtered by the stray inductance and parasitic capacitance. The inverter and SC current harmonics look large. This is because the load is relatively small in this study, which aims at studying the impact of the current limit. At the rated load condition, the current harmonics are small, and their THD values are both below 5%.

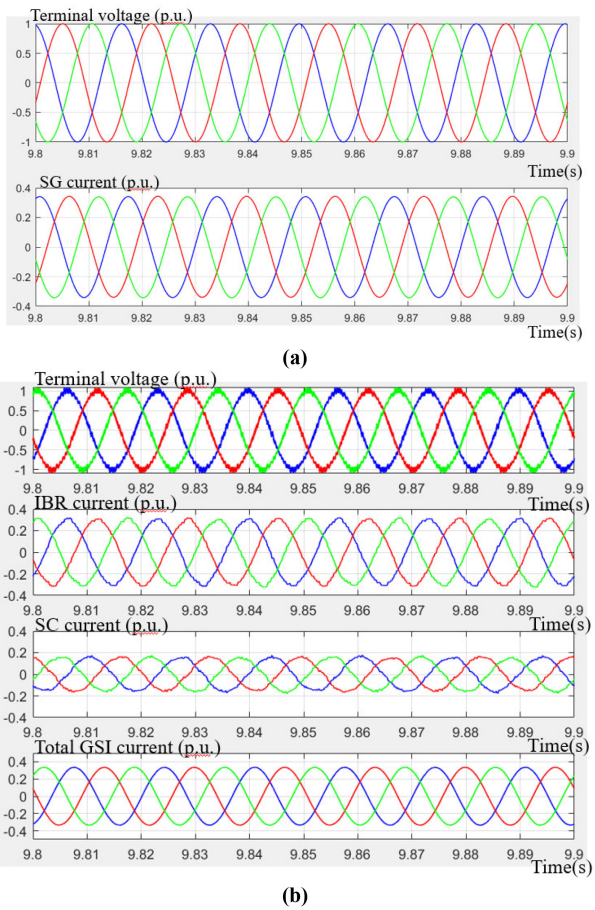

FIGURE 10. Terminal voltage and current waveforms in the steady-state operation of (a) the SGBR case and (b) the GSI case.

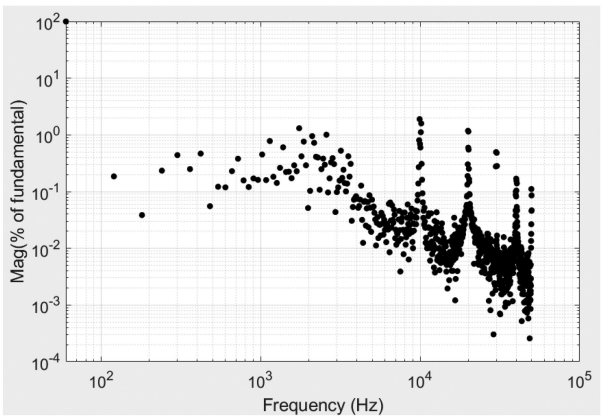

FIGURE 11. GSI terminal voltage harmonic spectrum.

B. DIFFERENT GRID FAULTS

After the steady-state operation, fault transients are studied. As shown in Table 3, different fault conditions, including three different fault types and six different fault resistances, are considered.

The three-phase fault with 0.1 p.u. fault resistance is taken as an example to show the detailed performance comparison between the SGBR case and the GSI case. In both cases, the fault happens at 10 s and lasts for 10 cycles (~0.17 s).

TABLE 3. Different Fault Conditions

Fault type	Fault resistance
Single phase-to-ground fault	0.01 p.u. 0.1 p.u. 0.3 p.u. 0.6 p.u. 1.0 p.u. 3.0 p.u.
Phase-to-phase fault	
Three-phase fault	

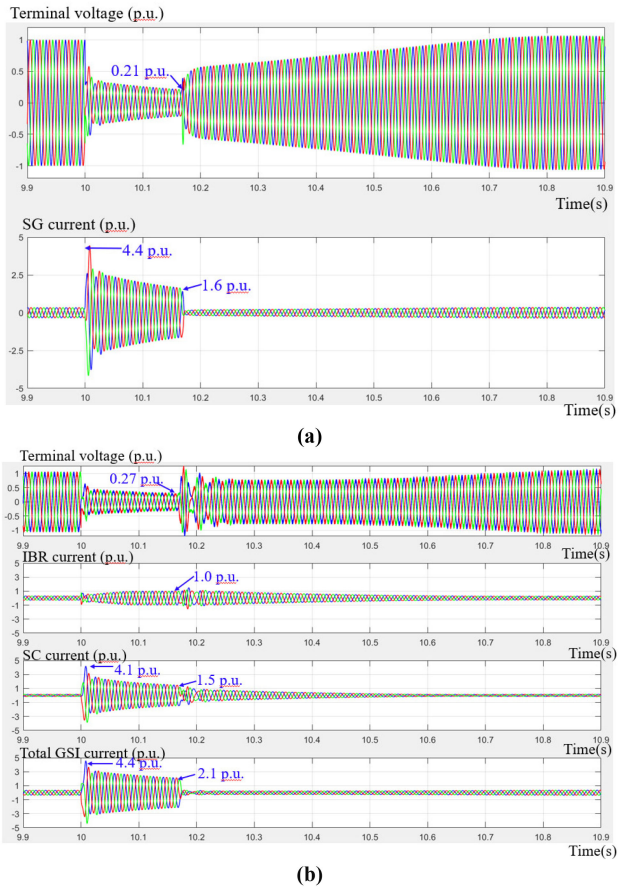

FIGURE 12. Terminal voltage and current waveforms in the three-phase fault with 0.1 p.u. fault resistance in (a)the SGBR case and (b)the GSI case.

The terminal voltage and current waveforms in the SGBR and GSI cases are shown in Fig. 12(a) and (b), respectively. During the fault period, the terminal voltage dropped in both SGBR and GSI cases, but the GSI has a slightly higher voltage. The SG current and the GSI total current start with the same peak and then decreases, but the GSI has a slower decreasing rate so that it has a 0.5 p.u. higher current at the end of the fault period. Because of the current contribution from the IBR, the current provided by the SC is smaller than the current provided by the SG. As a result, the SC exhibits slightly higher terminal voltage because of less internal voltage drop.

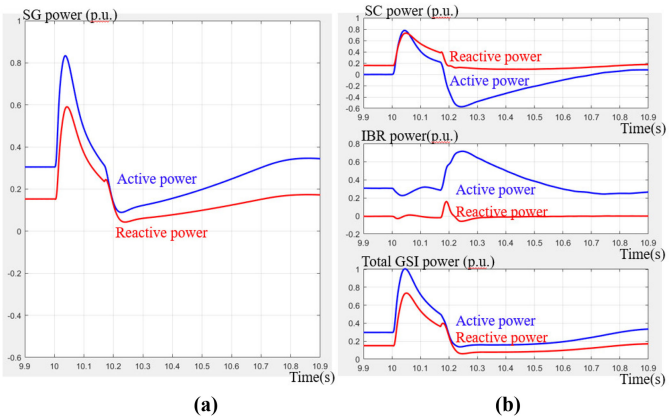

FIGURE 13. Power curves in the three-phase fault with 0.1 p.u. fault resistance in (a)the SGBR case and (b)the GSI case.

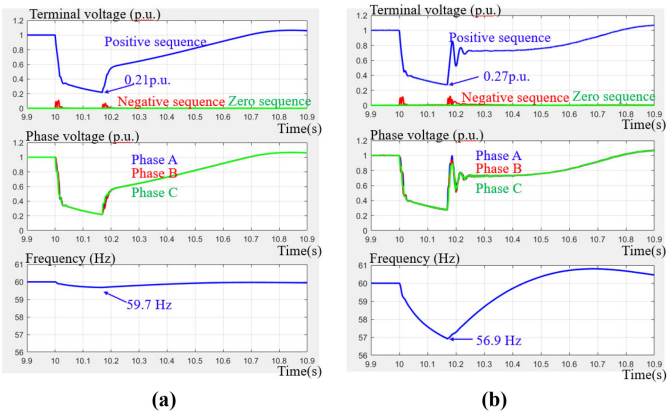

FIGURE 14. Terminal voltage and frequency in the three-phase fault with 0.1 p.u. fault resistance in (a)the SGBR case and (b)the GSI case.

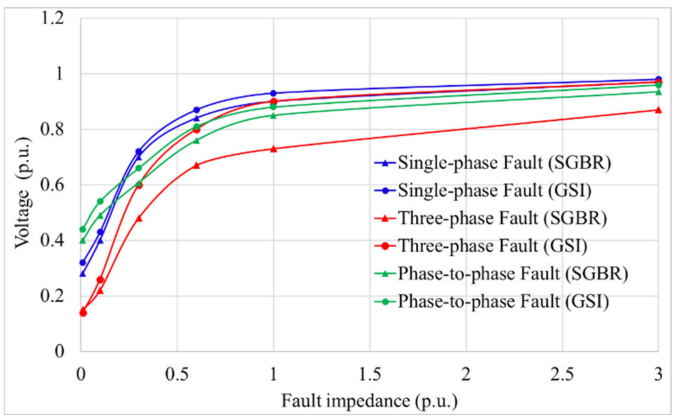

FIGURE 15. Minimum voltage during the fault period in different fault conditions.

Besides, it can be found that the IBR reaches its current limit, i.e., 1 p.u during the fault period.

Therefore, the proposed GSI outputs more overcurrent than the conventional SG during the fault period. To perform similar to an SGBR, the GSI only needs to provide a similar overcurrent, so a smaller SC could be used, depending on the system need.

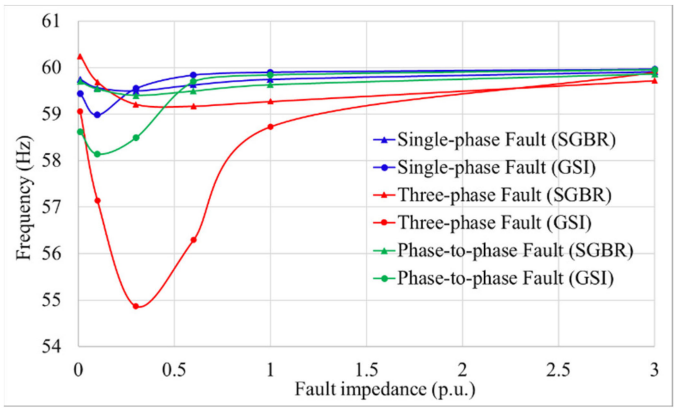

FIGURE 16. Frequency nadir during the fault period in different fault conditions.

The active and reactive power waveforms in the SGBR and GSI cases are shown in Fig. 13(a) and (b), respectively. When the fault happens, both the SG and the SC output more reactive power to support the terminal voltage. Besides, they also output more active power, which is from their kinetic energy (inertia), trying to support the frequency. However, because of the slow mechanical power input regulation of the SG and the lack of mechanical power input of the SC, both the SG and the SC slow down, which results in the frequency drop. As shown in Fig. 14(a) and (b), because of the smaller inertia constant, the GSI case has a larger frequency drop than the SGBR case. This can be solved by increasing the inertia of the SC, such as adding a flywheel, or by having an inverter with a larger current limit or overcurrent capability, which however needs to change the physical design of the inverter

From Fig. 13(b), during the fault period, the inverter's active power output is low due to the low terminal voltage and the inverter current limit. As shown in Fig. 13, after the fault is cleared, as the voltage recovers, the inverter outputs more active power to speed up the SC, and the frequency increases correspondingly. Fig. 14(a) and (b) also show the terminal voltages for positive and negative sequences, and for different phases. The GSI case has 0.06 p.u. higher voltage than the SG case, which has been discussed above.

The voltage performance comparison between the SGBR and the GSI under different fault conditions is shown in Fig. 15. The GSI cases have higher terminal voltages than their corresponding SGBR cases. Therefore, the proposed GSI setup can maintain the grid voltage at an even higher level during fault transients so that the system loads will not be affected. It can also be concluded that the GSI unit can output more overcurrent under the same system conditions. Again, the overcurrent level can be adjusted with a lower rating SC.

The frequency nadir during the fault period under different fault conditions is shown in Fig. 16. When the fault resistance is low (but near zero), the system consumes more active power during the fault. Because the SC has lower inertia than the

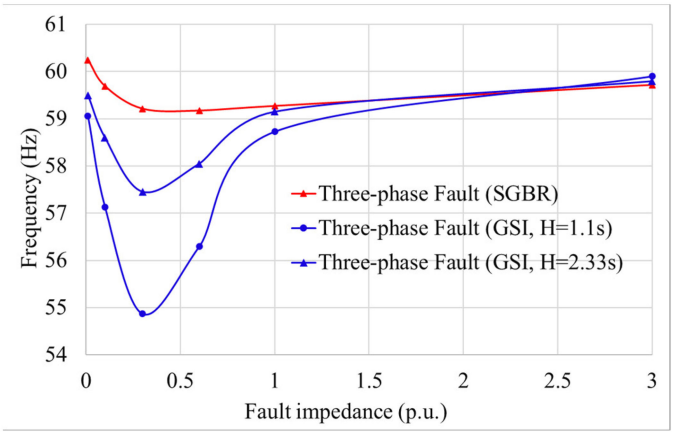

FIGURE 17. Frequency nadir comparison considering different SC inertia constants.

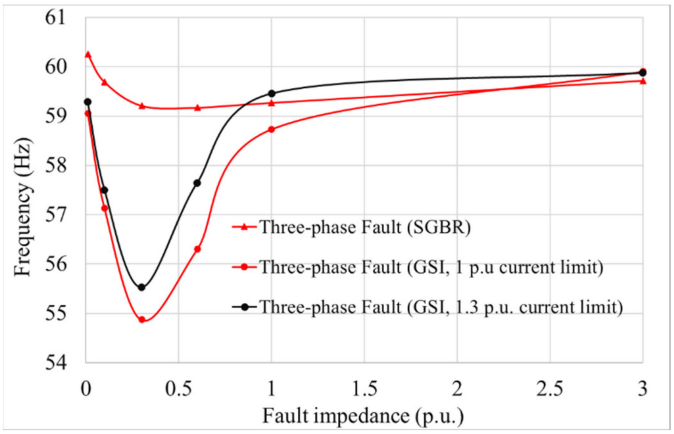

FIGURE 18. Frequency nadir during the fault period in terms of different IBR current limits (the SC inertia constant H=1.1 s).

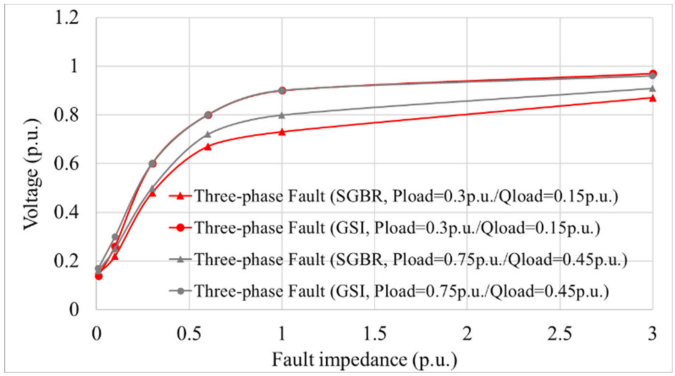

FIGURE 19. Minimum voltage during the fault period in terms of different system loads (the SC inertia constant H=1.1 s; inverter current limit is 1 p.u.).

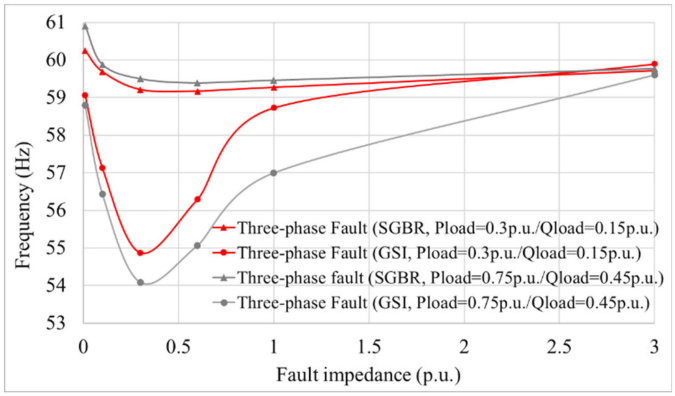

FIGURE 20. Frequency nadir during the fault period in terms of different system loads (the SC inertia constant H=1.1 s; inverter current limit is 1 p.u.).

SGBR, when the inverter reaches its current limit, the GSI has a lower frequency nadir than their corresponding SGBR case. However, when the fault resistance is large, the system does not consume much active power during fault. In this case, if the inverter does not hit its current limit, it can support all the active power for the external system and the SC, so the GSI has a larger frequency nadir than the SGBR.

C. IMPACT OF THE SC INERTIA

As discussed above, compared to the SGBR, the lower inertia constant of the SC results in a lower frequency nadir during the fault period. However, the inertia constant may vary in different machines, and the inertia constant of the SC can be increased with a flywheel or special mechanical design. Therefore, the impact of the SC inertia is studied. A higher SC inertia constant, 2.33 s, which is 1/3 of the SGBR inertia constant, is considered. As shown in Fig. 17, with higher inertia constant, the frequency nadir curve of the GSI is improved. If desired, the frequency performance of the GSI can be further improved by adding inertia to the SC, such as a flywheel, or by increasing the inverter current limit as will be discussed below.

D. IMPACT OF THE INVERTER CURRENT LIMIT

In the above conditions, the inverter current limit is set at 1 p.u., which is the lower boundary. Since the inverter mainly outputs active power to support the terminal voltage frequency, the current limit impacts the maximum active power output during the transient and therefore impacts frequency performance. As shown in Fig. 18, a higher inverter current limit will lead to a lower frequency drop with a larger available active power.

E. IMPACT OF SYSTEM LOADS

To evaluate the impact of system load level, three system loads, L_1, L_2, and L_3, are changed all to 0.25 p.u. active power and 0.15 p.u. reactive power. Therefore, the system has a total load of 0.75 p.u. active power and 0.45 p.u. reactive power. The comparison studies are conducted in three-phase fault conditions. As shown in Fig. 19, the SGBR case with a larger load shows a little lower voltage drop because its field current and internal back-emf are higher; however, the two GSI cases

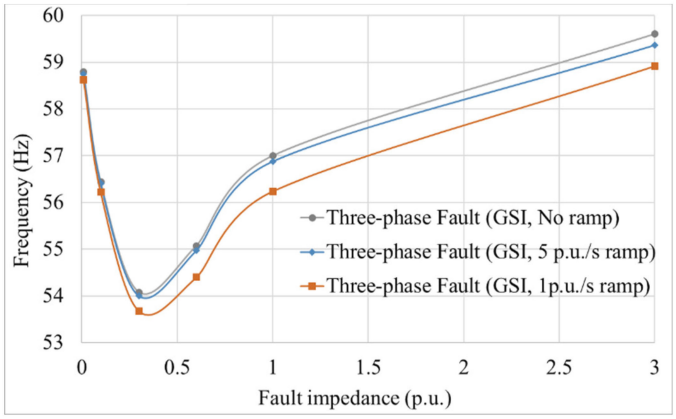

FIGURE 21. Frequency nadir during the fault period in terms of different inverter current ramp speeds (the SC inertia constant H=1.1 s; inverter current limit is 1 p.u.; system loads are 0.75 p.u. active power and 0.45 p.u. reactive power).

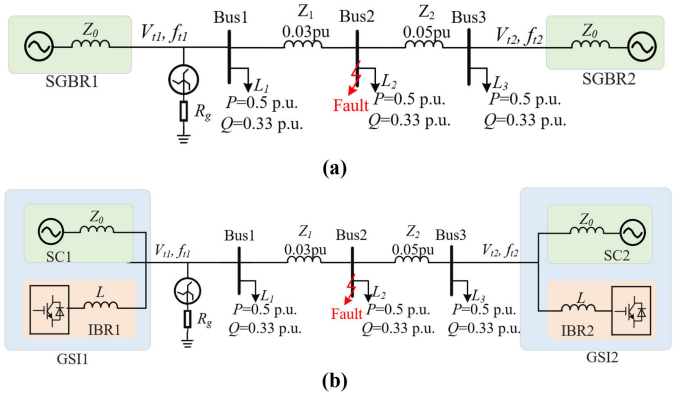

FIGURE 22. Two-unit operation system configuration of (a) the SGBR case and (b) the GSI case.

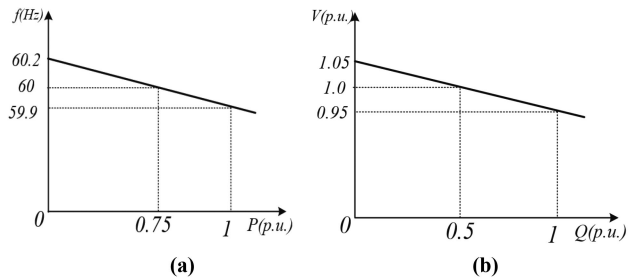

FIGURE 23. Droop curves of (a) frequency and (b) voltage.

do not show much difference because their SC field current and internal back-emf differences are much smaller than those of the SGBR cases.

The comparison of the frequency nadirs during the fault period is shown in Fig. 20. With a larger system load, the SGBR case has a larger frequency nadir, because of the overall active power difference between the fault period and the steady state is smaller. For the GSI cases, however, a higher system load leads to a smaller frequency nadir because of less inverter current margin for frequency support.

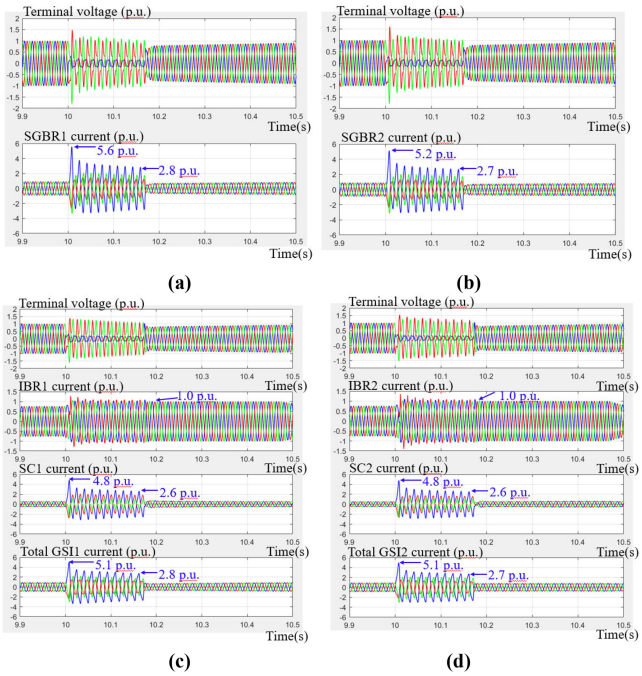

FIGURE 24. Terminal voltage and current waveforms during the single phase-to-ground fault in (a) SGBR1, (b) SGBR2, (c) GSI1, and (d) GSI2.

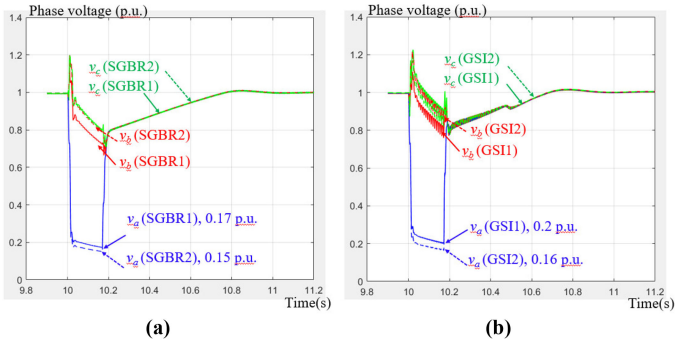

FIGURE 25. Phase voltage waveforms during the single phase-to-ground fault in (a) the SGBR case and (b) the GSI case.

F. IMPACT OF THE INVERTER CURRENT RAMP

In practice, the energy resource of the IBR has a power change rate limit. As a result, the inverter current cannot change instantaneously. To evaluate the impact, a current ramp is added to the inverter's current reference input. Three different current ramp rates: no ramp (used in the above conditions), 5 p.u./s, and 1 p.u./s, are taken into consideration. This limitation has little impact on the voltage performance but has an impact on the frequency performance. As shown in Fig. 21, a slower current ramp rate leads to a larger frequency drop during the fault period. The impact of the current ramp rate on the frequency performance is relatively small. If desired, faster energy resources such as battery energy storage can be used to improve the ramp rate.

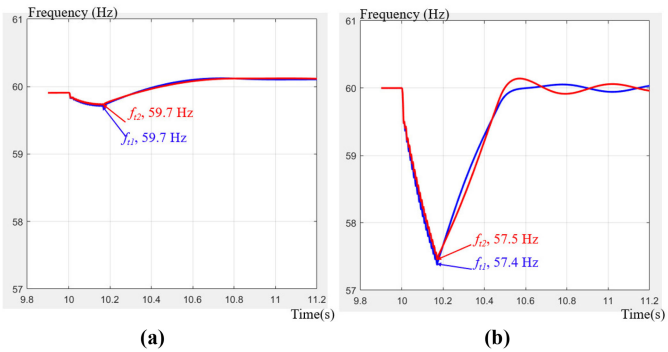

FIGURE 26. Frequency waveforms during the single phase-to-ground fault in (a) the SGBR case and (b) the GSI case.

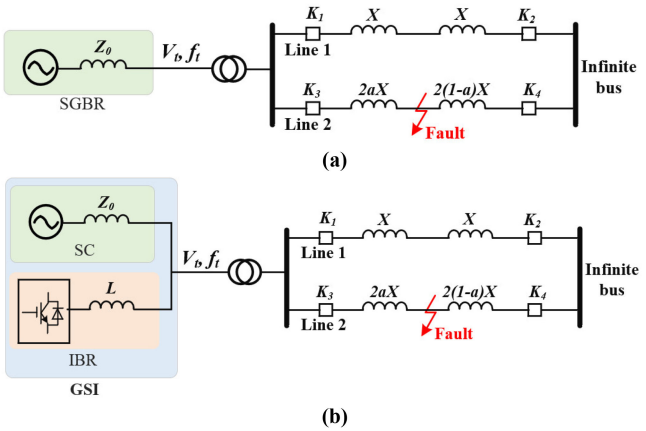

FIGURE 27. Transient stability study configuration of (a)the SGBR case and (b)the GSI case.

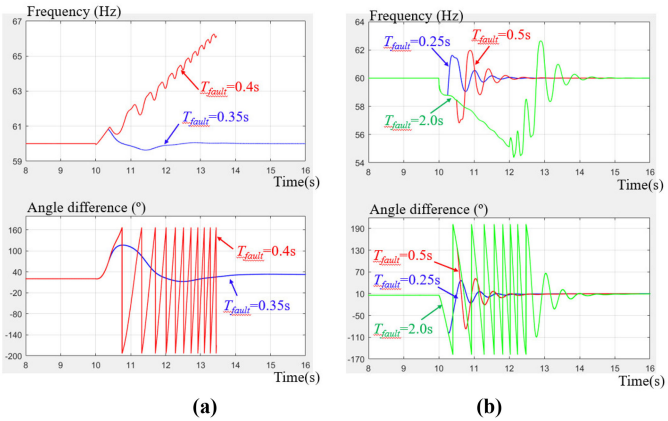

FIGURE 28. Frequency and angle waveforms of (a) the SG case and (b) the GSI case.

IV. MULTIPLE-UNIT OPERATION

In a large power system, multiple generation units operate together. A two-unit system is taken as an example to evaluate the performance of multiple proposed GSIs. The system configurations of the SGBR case and the GSI case are shown in Fig. 22(a) and (b), respectively. Two generation units are connected at the two ends of the power grid, which has three buses, and the line impedances of Bus1 to Bus2 and Bus2 to Bus 3 are 0.03 p.u. and 0.05 p.u., respectively. All buses have identical loads: 0.5 p.u. active power and 0.33 p.u. reactive power, so the total system load is 1.5 p.u. active power and 1 p.u. reactive power. Each generation unit operates individually, and no communication is needed. To realize the active and reactive power sharing between the two generation units, the voltage and frequency droop curves shown in Fig. 23(a) and (b) are adopted.

A single-phase-to-ground fault is applied on Bus 2 at 10 s. It lasts for 10 cycles and is then automatically cleared. Comparisons between the SGBR and GSI cases, and between the GSI1 and GSI2 are conducted.

The terminal voltage and current waveforms of SGBR1, SGBR2, GSI1, and GSI2 are shown in Fig. 24(a), (b), (c), and (d), respectively. In both the SGBR case and the GSI case, the two generation units share both the steady-state and transient currents, which verifies the multi-unit operation of the proposed GSI. Also, during the fault transient, although the SC outputs a little smaller current than the SG, the total output currents of the GSI units are similar to those of the SGBR units, which verifies the overcurrent capability of the proposed GSI in multi-unit operation.

The phase voltage waveforms of the SGBR case and GSI case are shown in Fig. 25(a) and (b), respectively. During both the steady state and the fault transient, the two GSI units have similar terminal voltages. Also, the three-phase voltages in the GSI case are slightly higher than those in the SGBR case. The observation is the same as in the single-unit operation.

The frequency performances of the SGBR case and GSI case are shown in Fig. 26(a) and (b), respectively. The two generation units have similar frequency waveforms, and the slight difference is due to the different line impedances. Moreover, similar to the single-unit operation, the GSI case has a larger frequency drop during the fault period due to lower SC inertia and the inverter current limit, compared to the SGBR case.

V. TRANSIENT STABILITY PERFORMANCE

The transient stability performance is another key point for the proposed GSI. A comparison is conducted between the SGBR and the GSI with a system configuration shown in Fig. 27(a) and (b), respectively. The generation unit, the SGBR or GSI, transfers energy to the infinite bus through two transmission lines, i.e., Line 1 and Line 2. Each transmission line has an impedance of $2X$. A three-phase fault is applied on Line 2 for a certain period, T_{fault}, which corresponds to the fault clearing time. Then, the fault is cleared through the operation of switches K_3 and K_4. Therefore, after the fault is cleared, Line 2 is disconnected and only Line 1 can deliver power. The location of the fault is determined by the location factor, a, which is between 0 and 1.

An example is taken to show the difference in the transient stability performance between the SGBR and the GSI. In both cases, the line impedance X=0.1 p.u. and the location factor a=0.03, which means the fault happens close to the

generation unit bus. Based on the classical swing equation and the mechanical equation of the SGBR [34], the critical clearing time is around 0.35 s, so 0.35 s and 0.4 s fault clearing times are applied, respectively, to the SGBR case. As shown in Fig. 28(a), with 0.35 s fault clearing time, the SGBR does not have the transient stability issue. The angle difference between the SG and the infinite bus increases from 19° to 116° and then goes back to 32° in the post-fault steady state. At the same time, the frequency increases to 60.8 Hz and then goes back to 60 Hz. However, with 0.4 s fault clearing time, the SG frequency keeps increasing, losing synchronism with the infinite bus even after the fault is cleared.

The GSI, however, performs in a quite different way than the SGBR. As shown in Fig. 28(b), three different fault clearing times, 0.25 s, 0.5 s, and 2.0 s, are applied, and the GSI does not exhibit the transient stability issue in all three cases. Although during the fault period, the SC loses synchronism with the infinite bus, after the fault is cleared it can reestablish the synchronism, even with a quite long fault clearing time, such as 2.0 s.

Another difference between the GSI and SGBR is that the frequency in the SGBR case increases during the fault period, while it decreases in the GSI case. The fundamental difference is that the SC does not have a mechanical power input as the SG. When a fault happens, the SC may not get sufficient active power to compensate for its power losses and keep rotating at the rated speed. As a result, the SC will slow down, and the frequency will drop. When the fault is cleared, even though the SC rotating speed is low (so is the frequency), the IBR can output more active power to speed it up, and the frequency will eventually go back to the reference. Then, the synchronism between the GSI unit and the infinite bus can be reestablished. Therefore, it can be concluded that the GSI does not have transient stability issues. Again, although the frequency drop in the GSI case is larger, it can be improved by increasing the inertia of the SC.

VI. DISCUSSION

This paper has demonstrated the importance of the overcurrent capability of GFM IBRs during short circuit transients, and proposed and validated through simulation the GSI concept and its control method in grid forming operation. The GSI provides a relatively simple solution for providing overcurrent capability based on the available inverter and SC technologies, with changes needed only for their control. Several aspects related to the design and operation of the GSI are not considered and need to be further investigated in future work.

1) The system-level design of the GSI. Not all IBRs in the system need to work in the GFM mode or need to provide overcurrent capability. Therefore, some IBR does not need to have an SC. Instead, the GSI can be implemented based on the system level needs from a system study, which needs to be performed anyway when installing a generation source
2) Adding an SC to an IBR will add cost, just like any other solution to provide overcurrent capability. As mentioned earlier, if other more cost-effective overcurrent sources become available, they can be used instead to replace the SC or the GSI. One such potential solution is only to use IBR with energy storage and an oversized inverter. However, today's grid-tied inverters are not designed to provide only transient overcurrent capability. Over-sizing inverters based on the rated current will likely be noneconomical and not necessary since grid transients are mostly short in time. One potential future work is to develop a cost-effective inverter with five to ten times transient overcurrent capability. In addition, a new IBR inverter design approach is desired for this type of inverter.
3) The SC rating selection and the IBR inverter current limit setting. As one unit, the GSI's overcurrent is shared between the SC and the IBR inverter. The selection of the SC rating and the inverter current limit also needs to be studied to get a better performance considering system performance like inertia, grid strength, and the overall cost.
4) The impact of the SC ratings and parameters. The SC does not need to have the same rating as the SG, which is an assumption in this paper for comparison purposes. Instead, the ratings of the SC can be designed to have more or less inertia, to provide more or less transient overcurrent, etc.
5) The impact of the energy resources. The energy resources could be PV, wind, fuel cell, etc. Since they have different characteristics, for example, the power ramp rates, the design of the GSI for them could be different.
6) Experimental testing. Since this work focuses on control using the well-known IBR, SC, and SG models, simulation should be sufficient to validate the method. For eventual experimental validation, full-scaled SC and SG are needed as their small-scaled counterparts do not represent the large machine transient behaviors well.

VII. CONCLUSION

In this paper, a GSI setup is proposed, which combines a current-limited IBR with a co-located SC, to provide an overcurrent comparable to an SGBR. Different from the existing use of SCs, which are installed in the system and operated independently to provide overcurrent and inertia, the proposed GSI scheme combines the SC and the IBR at the source side to provide grid forming functions, including the overcurrent from the integrated generation source. The terminal voltage is controlled by the SC through its excitation control, and the frequency is controlled by the IBR through its active power control.

The performance of the proposed GSI is confirmed through the simulation comparison studies between the GSI and the SGBR in steady-state operation, different grid fault conditions, multiple-unit operation, as well as transient stability performance. It is found that the GSI can provide a similar or

slightly higher overcurrent than its SGBR counterpart. With the available overcurrent capability, the grid transient voltage supported by the GSI will be more than adequate compared with the SG. It can also be concluded that the system protection and black start will not be impacted. Moreover, the proposed GSI setup does not exhibit any transient stability issues; even after a long fault duration, the GSI can reestablish the synchronism. Due to the smaller SC inertia constant, the frequency variation of the GSI is larger than that of the SGBR when the inverter current is limited to 1 p.u. However, if the frequency drop variation is not in an acceptable range, it can be improved by adding inertia to the SC and/or by allowing a small overcurrent for the inverter. Also, the proposed GSI and its control can be easily extended to multiple units, and frequency and voltage droop control can be adopted to achieve power sharing among different units.

REFERENCES

[1] Y. Lin et al., "Research roadmap on grid-forming inverters," National Renewable Energy Lab.(NREL), Golden, CO, USA, Tech. Rep. NREL/TP-5D00-73476, 2020.

[2] J. Matevosyan et al., "Grid-forming inverters: Are they the key for high renewable penetration?," *IEEE Power Energy Mag.*, vol. 17, no. 6, pp. 89–98, Nov./Dec. 2019.

[3] R. Rosso, X. Wang, M. Liserre, X. Lu, and S. Engelken, "Grid-forming converters: An overview of control approaches and future trends," in *Proc. IEEE Energy Convers. Congr. Expo.*, 2020, pp. 4292–4299.

[4] P. Unruh, M. Nuschke, P. Strauß, and F. Welck, "Overview on grid-forming inverter control methods," *Energies*, vol. 13, no. 10, 2020, Art. no. 2589.

[5] L. Toma et al., "On the virtual inertia provision by BESS in low inertia power systems," in *Proc. IEEE Int. Energy Conf.*, 2018, pp. 1–6.

[6] Q. Peng, Y. Yang, T. Liu, and F. Blaabjerg, "Coordination of virtual inertia control and frequency damping in PV systems for optimal frequency support," *CPSS Trans. Power Electron. Appl.*, vol. 5, no. 4, pp. 305–316, 2020.

[7] L. Haifeng, W. Fan, J. Tao, and X. Guoyi, "Parameter tuning method of virtual inertia controller of wind turbines considering wind power fluctuation," in *Proc. 5th Asia Conf. Power Elect. Eng.*, 2020, pp. 533–537.

[8] U. Tamrakar, D. Shrestha, M. Maharjan, B. P. Bhattarai, T. M. Hansen, and R. Tonkoski, "Virtual inertia: Current trends and future directions," *Appl. Sci.*, vol. 7, no. 7, 2017, Art. no. 654.

[9] D. B. Rathnayake et al., "Grid forming inverter modeling, control, and applications," *IEEE Access*, vol. 9, pp. 114781–114807, 2021.

[10] *IEEE Recommended Practice for Powering and Grounding Electronic Equipment*, IEEE Standard1100-2005 (Revision of IEEE Standard 1100-1999), pp. 1–703, 2006.

[11] "*IEEE Recommended Practice for Voltage Sag and Short Interruption Ride-Through Testing for End-Use Electrical Equipment Rated Less Than 1000 V*," IEEE Standard 1668-2017 (Revision of IEEE Standard 1668-2014), pp. 1–85, 2017.

[12] D. Lepour, M. Paolone, G. Denis, C. Cardozo, T. Prevost, and E. Guiu, "Performance assessment of synchronous condensers vs voltage source converters providing grid-forming functions," in *Proc. IEEE Madrid PowerTech*, 2021, pp. 1–6.

[13] J. Shiles et al., "Microgrid protection: An overview of protection strategies in North American microgrid projects," in *Proc. IEEE Power Energy Soc. Gen. Meeting*, 2017, pp. 1–5.

[14] T. Patel, S. Brahma, J. Hernandez-Alvidrez, and M. J. Reno, "Adaptive protection scheme for a real-world microgrid with 100% inverter-based resources," in *Proc. IEEE Kansas Power Energy Conf.*, 2020, pp. 1–6.

[15] M. A. Aftab, S. M. S. Hussain, I. Ali, and T. S. Ustun, "Dynamic protection of power systems with high penetration of renewables: A review of the traveling wave based fault location techniques," *Int. J. Elect. Power Energy Syst.*, vol. 114, 2020, Art. no. 105410.

[16] H. Jain, G. -S. Seo, E. Lockhart, V. Gevorgian, and B. Kroposki, "Black-start of power grids with inverter-based resources," in *Proc. IEEE Power Energy Soc. Gen. Meeting*, 2020, pp. 1–5.

[17] T. Qoria, F. Gruson, F. Colas, X. Kestelyn, and X. Guillaud, "Current limiting algorithms and transient stability analysis of grid-forming VSCs," *Electric Power Syst. Res.*, vol. 189, 2020, Art. no. 106726.

[18] L. Zhang, L. Harnefors, and H. Nee, "Power-synchronization control of grid-connected voltage-source converters," *IEEE Trans. Power Syst.*, vol. 25, no. 2, pp. 809–820, May 2010.

[19] Y. Ma, F. Wang, and L. M. Tolbert, "Virtual synchronous generator with limited current–impact on system transient stability and its mitigation," in *Proc. IEEE Energy Convers. Congr. Expo.*, 2020, pp. 2773–2778.

[20] E. Rokrok, T. Qoria, A. Bruyere, B. Francois, and X. Guillaud, "Transient stability assessment and enhancement of grid-forming converters embedding current reference saturation as current limiting strategy," *IEEE Trans. Power Syst.*, vol. 37, no. 2, pp. 1519–1531, Mar. 2022.

[21] Y. Katsuya, Y. Mitani, and K. Tsuji, "Power system stabilization by synchronous condenser with fast excitation control," in *Proc. Int. Conf. Power System Technol.*, 2000, vol. 3, pp. 1563–1568.

[22] C. V. Thio and J. B. Davies, "New synchronous compensators for the nelson river HVDC system-planning requirements and specification," *IEEE Trans. Power Del.*, vol. 6, no. 2, pp. 922–928, Apr. 1991.

[23] A. Stiger, R. A. Rivas, and M. Halonen, "Synchronous condensers contribution to inertia and short circuit current in cooperation with STATCOM," in *Proc. IEEE PES GTD Grand Int. Conf. Expo. Asia*, 2019, pp. 955–959.

[24] H. T. Nguyen, G. Yang, A. H. Nielsen, and P. H. Jensen, "Combination of synchronous condenser and synthetic inertia for frequency stability enhancement in low-inertia systems," *IEEE Trans. Sustain. Energy*, vol. 10, no. 3, pp. 997–1005, Jul. 2019.

[25] A. Di Giulio et al., "Increased grid performance using synchronous condensers in multi in-feed multi-terminal HVDC system," in *Proc. CIGRE Conf. Paper*, 2014, Paper A1–112.

[26] F. B. K. Mahmood et al., "Weakest location exploration in IEEE-14 bus system for voltage stability improvement using STATCOM, synchronous condenser and static capacitor," in *Proc. Int. Conf. Elect., Comput. Commun. Eng.*, 2017, pp. 623–629.

[27] J. Jia, G. Yang, A. H. Nielsen, and V. Gevorgian, "Investigation on the combined effect of VSC-based sources and synchronous condensers under grid unbalanced faults," *IEEE Trans. Power Del.*, vol. 34, no. 5, pp. 1898–1908, Oct. 2019.

[28] R. W. Kenyon, A. Hoke, J. Tan, and B. Hodge, "Grid-Following inverters and synchronous condensers: A grid-forming pair?," in *Proc. Clemson Univ. Power Syst. Conf.*, 2020, pp. 1–7.

[29] J. Jia, G. Yang, A. H. Nielsen, E. Muljadi, P. Weinreich-Jensen, and V. Gevorgian, "Synchronous condenser allocation for improving system short circuit ratio," in *Proc. 5th Int. Conf. Electric Power Energy Convers. Syst.*, 2018, pp. 1–5.

[30] E. Marrazi, G. Yang, and P. Weinreich-Jensen, "Allocation of synchronous condensers for restoration of system short-circuit power," *J. Modern Power Syst. Clean Energy*, vol. 6, no. 1, pp. 17–26, 2018.

[31] A. K. Morya, A. Shukla, and S. Doolla, "Control of grid connected cascaded H-bridge multilevel converter during grid voltage unbalance for photovoltaic application," in *Proc. IECON 39th Annu. Conf. IEEE Ind. Electron. Soc.*, 2013, pp. 7990–7995.

[32] W. Zhao, H. Choi, G. Konstantinou, M. Ciobotaru, and V. G. Agelidis, "Cascaded H-bridge multilevel converter for large-scale PV grid-integration with isolated DC-DC stage," in *Proc. 3rd IEEE Int. Symp. Power Electron. Distrib. Gener. Syst.*, 2012, pp. 849–856.

[33] J. Liu, M. Yushi, T. Ise, J. Yoshizawa, and K. Watanabe, "Parallel operation of a synchronous generator and a virtual synchronous generator under unbalanced loading condition in microgrids," in *Proc. IEEE 8th Int. Power Electron. Motion Control Conf.*, 2016, pp. 3741–3748.

[34] P. Kundur, N. J. Balu, and M. G. Lauby, *Power System Stability and Control*, vol. 7, New York, NY, USA: McGraw-Hill, 1994.

[35] W. E. Corporation, *Electrical Transmission and Distribution Reference Book*. Pittsburgh, PA, USA: Westinghouse Electric Corporation, 1964.

[36] "*IEEE Recommended Practice for Excitation System Models for Power System Stability Studies*," IEEE Standard 421.5-2016 (Revision of IEEE Standard 421.5-2005), pp. 1–207, 2016.

[37] "*IEEE Recommended Practice and Requirements for Harmonic Control in Electric Power Systems*," IEEE Standard 519-2014 (Revision of IEEE Standard 519-1992), pp. 1–29, 2014.

HAIGUO LI (Member, IEEE) received the B.S. and M.S. degrees in electrical engineering from Shanghai Jiao Tong University, Shanghai, China, in 2014, and the Ph.D. degree in electrical engineering from the University of Tennessee, Knoxville, TN, USA, in 2017 and 2022, respectively. Since 2022, he has been a Research Assistant Professor with the Department of Electrical Engineering and Computer Science, The University of Tennessee.

His research interests include grid-connected converter design, control and test, MV SiC device application in grid power electronics, MV converter design and control, and MV gate driver power supply.

CHENG NIE (Member, IEEE) was born in Hubei, China, in 1985. He received the B.S. degree from Hunan University, Changsha, China, in 2008, and the M.S. and Ph.D. degrees from Xi'an Jiaotong University, Xi'an, China, in 2011 and 2018, respectively. From 2019 to 2021, he joined the University of Tennessee, Knoxville, TN, USA, as a Postdoctoral Research Associate. Since 2021, he has been a System Engineer with the TBEA Xi'an Electric Technology Co. LTD, Xi'an, China. His research interests include wide bandgap devices, modular multilevel converters, solid-state transformers, microgrids, and renewable energy.

FRED WANG (Fellow, IEEE) received the B.S. degree in electrical engineering from Xi'an Jiaotong University, Xi'an, China, in 1982, and the M.S. and Ph.D. degrees in electrical engineering from the University of Southern California, Los Angeles, CA, USA, in 1985 and 1990, respectively.

From 1990 to 1992, he was a Research Scientist with Electric Power Lab, University of Southern California. In 1992, he joined the GE Power Systems Engineering Department, Schenectady, NY, USA, as an Application Engineer. From 1994 to 2000, he was a Senior Product Development Engineer with GE Industrial Systems, Salem, VA, USA. During 2000–2001, he was the Manager of Electronic and Photonic Systems Technology Lab, GE Global Research Center, Schenectady, NY, USA, and Shanghai, China. In 2001, he joined the Center for Power Electronics Systems (CPES), Virginia Tech, Blacksburg, VA, USA, as a Research Associate Professor and became an Associate Professor in 2004. From 2003 to 2009, he was the CPES Technical Director. Since 2009, he has been with The University of Tennessee, Knoxville, TN, USA, and Oak Ridge National Lab, Knoxville, TN, USA, as a Professor and the Condra Chair of Excellence in power electronics. He is a Founding Member and the Technical Director of the multi-university NSF/DOE Engineering Research Center for Ultra-Wide-Area Resilient Electric Energy Transmission Networks (CURENT), led by The University of Tennessee. His research interests include power electronics and power systems. Dr. Wang is a Fellow of the U.S. National Academy of Inventors.